Extraction of the distribution function $h_{1T}^{\perp}$ from experimental data

Christopher Lefky and Alexei Prokudin

Extraction of the distribution function $h_{1T}^\perp$ from experimental data

Christopher Lefky[1, *] and Alexei Prokudin[2, †]

[1] *Creighton University, Omaha, NE*
[2] *Jefferson Lab, 12000 Jefferson Avenue, Newport News, Virginia 23606, USA*
(Dated: Friday 16th January, 2015)

We attempt an extraction of the pretzelosity distribution ($h_{1T}^\perp$) from preliminary COMPASS, HER-MES, and JLAB experimental data on $\sin(3\phi_h - \phi_S)$ asymmetry on proton, and effective deuteron and neutron targets. The resulting distributions, albeit big errors, for the first time show tendency for up quark pretzelosity to be positive and down quark pretzelosity to be negative. A model relation of pretzelosity distribution and Orbital Angular Momentum of quarks is used to estimate contributions of up and down quarks.

PACS numbers: 13.88.+e, 13.85.Ni, 13.60.-r, 13.85.Qk

I. INTRODUCTION

The proton is a very intricate dynamical system of quarks and gluons. Spin decomposition and partonic structure of the nucleon remain key problems of modern nuclear physics and Orbital Angular Momentum (OAM) of partons emerged as an essential part of our understanding of the internal structure of the nucleon. Studying the structure of the proton is one of the main goals of many past and present experimental facilities and experiments such as H1 (DESY), ZEUS (DESY), HERMES (DESY), COMPASS (CERN), Jefferson Lab, RHIC (BNL), various Drell-Yan experiments [1], and e^+e^- annihilation experiments by Belle and BaBar Collaborations. Future Jefferson Lab 12 [2] and EIC [3] are going to provide very detailed experimental data that will improve our knowledge of hadron structure in valence and sea regions. Description of Semi-Inlcusive Deep Inelastic Scattering (SIDIS), e^+e^- annihilation to two hadrons, and Drell-Yan process at low transverse momentum (with respect to the resolution scale) of observed particles is achieved in terms of the so-called Transverse Momentum Dependent distribution and fragmentation functions (collectively called TMDs). TMDs depend on longitudinal momentum fraction and on transverse motion vector of patrons inside of the nucleon and thus allow for a three-dimensional "3-D" representation of the nucleon structure in momentum space and are related to Orbital Angular Momentum (OAM) of partons.

One particular Transverse Momentum Dependent (TMD) distribution function might play a particular role in our understanding of the spin of the nucleon. This distribution is called pretzelosity ($h_{1T}^\perp$) and its name stems from the fact that a polarized proton is not spherically symmetric [4]. This function depends on the fraction of hadron momentum carried by the parton, x, and the intrinsic transverse momentum of the parton, $\boldsymbol{k}_\perp$, and corresponds to a quadrupole modulation of parton density in the distribution of transversely polarized quarks in a transversely polarized nucleon [5–7]

$$\Phi^{[i\sigma^{\alpha+}\gamma_5]}(x, \boldsymbol{k}_\perp) = S_T^\alpha\, h_1(x, k_\perp^2) + S_L\, \frac{k_\perp^\alpha}{M}\, h_{1L}^\perp(x, k_\perp^2) - \frac{k_\perp^\alpha k_\perp^\rho - \frac{1}{2}\, k_\perp^2\, g_T^{\alpha\rho}}{M^2}\, S_{T\rho} h_{1T}^\perp(x, k_\perp^2) - \frac{\epsilon_T^{\alpha\rho} k_{\perp\rho}}{M} h_1^\perp(x, k_\perp^2). \quad (1)$$

In this formula S_T and S_L are transverse and longitudinal components of polarsation vector and other functions that enter in the projection of parton density with $\sigma^{\alpha+}\gamma_5$ are transversity [8] (h_1), Boer-Mulders function [9] ($h_1^\perp$), and so-called worm-gear or Kotzinian-Mulders function [10] ($h_{1L}^\perp$). As one can see, the pretzelosity distribution enters with $k_\perp^\alpha k_\perp^\rho - \frac{1}{2}\, k_\perp^2\, g_T^{\alpha\rho}$ coefficient that corresponds to a quadrupole modulation of parton density in momentum space. The pretzelosity distribution in convolution with the Collins fragmentation function [11] generates $\sin(3\phi_h - \phi_S)$ asymmetry in Semi-Inclusive Deep Inelastic Scattering (SIDIS) and was studied experimentally by COMPASS [12–15] and HERMES [16–18] collaborations and JLAB [19]. We attempt the first extraction of pretzelosity from the latest experimental data [12–19] using extracted Collins fragmentation function from Ref. [20] for our analysis. we are going to use tree level approximation and neglect possible effects of TMD evolution (such as Sudakov suppression) in this paper and include only the relevant DGLAP evolution of collinear quantities. In fact, the span of Q^2 in the experimental data is narrow enough to assume small possible effects from evolution.

Model calculations of pretzelosity including bag and Light-Cone Quark model and predictions for experiments are presented in Ref. [21–27]. Note that most models predict negative u quark and positive d quark pretzelosity.

---

* ChristopherLefky@creighton.edu
† prokudin@jlab.org

In a vast class of models with spherically symmetric nucleon wave function in the rest frame, the pretzelosity distribution is related to OAM of quarks by the following relation [22, 27, 28]

$$\mathcal{L}_z^a = -\int dx\, d^2\mathbf{k}_\perp\, \frac{k_\perp^2}{2M^2} h_{1T}^{\perp a}(x, k_\perp^2) = -\int dx\, h_{1T}^{\perp(1)a}(x)\,. \tag{2}$$

It was shown in Ref. [29] that the relation of Eq. (2) did not correspond to intrinsic OAM of quarks. This relation is valid on amplitude level and not on operator level and may hold only numerically [29] as OAM is chiral and charge even, but pretzelosity is chiral and charge odd. We warn the reader that relation of Eq. (2) is model dependent and thus one cannot derive solid conclusions based on it, nevertheless it appears very interesting to attempt an extraction of the pretzelosity distribution ($h_{1T}^\perp$) from the experimental data on $\sin(3\phi_h - \phi_S)$ asymmetry and compare numerical results of Eq. (2) with existing calculations of OAM.

Lattice QCD results [30–32] using Ji's relation of Ref. [33] of the total angular momentum of flavor q contribution to the spin of the nucleon and GPDs H_q and E_q: $J_q = \frac{1}{2}\int dx\, x[H_q(x,0,0) + E_q(x,0,0)]$. Contribution of the quark spin is then subtracted from the result: $L_z^q = J_q - \frac{1}{2}\Sigma_q$. Refs. [30–32] use only the so-called connected insertions in lattice simulations and find the following result:

$$L_z^u < 0,\ L_z^d > 0,\ |L_z^{u+d}| \ll |L_z^u|, |L_z^d|\,. \tag{3}$$

Ref. [34] shows that, while $|L_z^{u+d}|$ largely cancels if only connected insertions are considered, the results change when disconnected insertions are included: their contributions are large and positive. Results of Ref. [34] at $Q^2 = 4$ GeV^2 imply that

$$L_z^u < 0,\ L_z^d > 0\,, \tag{4}$$

thus the smallness of the total $u + d$ contribution to the OAM is not confirmed. The connected insertions do not affect neither the difference $L_z^u - L_z^d$ nor the sign of L_z^u, L_z^d.

It is worth mentioning that TMDs exhibit the so-called generalized universality. Some TMDs may depend on the process. The most notorious examples are Sivers [9, 35] and Boer-Mulders [9] distributions that have opposite signs in SIDIS and DY [36–38]. Apart from the sign, these functions are the same and universal, however it turns out that there might be several universal functions corresponding to pretzelosity distribution. In particular, it was found in Ref. [39] that there are 3 different universal functions corresponding to pretzelosity. Those functions are in principle accessible in various processes, but one cannot distinguish them in SIDIS, thus we will use only one function $h_{1T}^\perp \equiv h_{1T}^{\perp\,\mathrm{SIDIS}}$.

As we mentioned previously, the relation of Eq. (2) OAM and pretzelosity function is a model inspired relation. It was shown that OAM is related to the so-called Generalised Transverse Momentum Dependent distributions (GTMDs), in particular to one denoted as $F_{1,4}$ [40]. There are two ways of construction OAM of quarks depending on the configuration of the gauge link in the operator definition: either canonical OAM of Jaffe-Manohar [41] in the spin decomposition $\frac{1}{2} = \frac{1}{2}\Delta\Sigma + L_z^q + \Delta G + L_z^g$ or kinetic OAM in the definition of Ji [33] in the spin decomposition $\frac{1}{2} = \frac{1}{2}\Delta\Sigma + L_z^q + J^g$. Definition of OAM in these two decomposition differs by the presence of derivative $i\partial$ in definition of Jaffe-Manohar [41] and covariant derivative $iD = i\partial - gA$ in the definition of Ji [33]. The presence of gauge field in kinetic OAM makes it different from canonical OAM. The relation of $F_{1,4}$ and OAM of patrons in longitudinally polarized nucleon was shown in Ref. [42] and model and QCD calculations of canonical and kinetic OAM were preformed in Refs. [43–45]. Results of Ref. [45] indicate that total kinetic OAM in a one quark model $L_z^q \sim (-0.04 \div -0.1)$ at $Q = 3$ GeV. Canonical and kinetic OAM were studied in Refs. [46] and the model results suggest that for u quark canonical $L_z^u = 0.11$ and kinetic $L_z^u = 0.13$ at the hadronic scale. The numerical difference between two definitions is generated by the presence of the gauge field, in models without gauge field term such as the scalar diquark model one obtains the same value for kinetic and canonical OAM [47]. Model results of Refs. [46, 47] are of opposite sign of lattice QCD results that suggest $L_z^u < 0$ and $L_z^d > 0$.

The rest of the paper is organized as follows: in Section II we will derive a general formula for the $A_{UT}^{\sin(3\phi_h - \phi_S)}$ single spin asymmetry associated with pretzelosity in TMD formalism. Formulas for unpolarized and polarized cross-sections will be presented in Sections II A and II B. We will calculate probability that existing experimental data from COMPASS, HERMES, and JLAB indicate that all pretzelosity functions are exactly equal to *zero*, i.e. the so-called null-signal hypothesis, in Section III. Then we attempt a detailed phenomenological fit of pretzelosity distributions in Section IV where we present resulting parameters of the fit of pretzelosity distributions and comparison with existing data. We will give predictions for future measurements at Jefferson Lab 12 in Section IV A. We will compare resulting pretzelosity distribution to models in Section V and test model relations on pretzelosity in Section VI. Using model relation of OAM of quarks and pretzelosity we will calculate OAM of up and down quarks in Section VII. Finally we will conclude in Section VIII.

II. $A_{UT}^{\sin(3\phi_h - \phi_S)}$ **SINGLE SPIN ASYMMETRY**

The part of the SIDIS cross section we are interested in reads [5, 7, 48]:

$$\frac{d\sigma}{dx\, dy\, d\phi_S\, dz\, d\phi_h\, dP_{hT}} = \frac{\alpha^2 2P_{hT}}{xy\, Q^2} \left\{ \left(1 - y + \frac{1}{2}y^2\right)(F_{UU,T} + \varepsilon F_{UU,L}) + S_T\,(1-y)\,\sin(3\phi_h - \phi_S)\,F_{UT}^{\sin(3\phi_h - \phi_S)} + ... \right\}$$

(5)

where one uses the following standard variables

$$x = \frac{Q^2}{2\,P\cdot q}, \quad y = \frac{P\cdot q}{P\cdot l}, \quad z = \frac{P\cdot P_h}{P\cdot q}, \quad \varepsilon \approx \frac{1-y}{1 - y + \frac{1}{2}y^2},$$

(6)

where α is the fine structure constant, $Q^2 = -q^2 = -(l - l')^2$ is the virtuality of the exchanged photon, P_{hT} is the transverse momentum of the produced hadron, S_T is transverse polarization, and ϕ_h, ϕ_S are the azimuthal angles of the produced hadron and the polarization vector with respect to the lepton scattering plane formed by l and l'. $F_{UU,L} = 0$ at $\mathcal{O}(k_\perp/Q)$ order of accuracy. Structure functions that we are interested in in this study are unpolarized structure function $F_{UU,T}$ and spin structure function $F_{UT}^{\sin(3\phi_h - \phi_S)}$, polarization state of the beam and target are explicitly denoted in definition of structure functions as "U"- unpolarised,"T"-transversely polarized. Ellipsis in Eq. (5) denotes contributions from other spin structure functions.

In this paper we will use the convention of Refs. [48–50] for the transverse momentum of incoming quark with respect to the proton's momentum and the hadron momentum with respect to the fragmenting quark:

$$\boldsymbol{k}_\perp, \, \boldsymbol{p}_\perp.$$

(7)

The advantage of this convention is that fragmentation function has probabilistic interpretation with respect to vector $\boldsymbol{p}_\perp$ i.e.

$$D_{h/a}(z) \equiv \int d^2\boldsymbol{p}_\perp D_{h/a}(z, p_\perp^2)\,.$$

(8)

The structure functions involved in Eq. (5) are convolutions of the distribution and fragmentation functions f and D [5, 7]

$$F_{AB} = \mathcal{C}[w\, f\, D],$$

(9)

where A, B indicate polarization state of beam and target U, L, T, and $\mathcal{C}[...]$ is defined as

$$\mathcal{C}[w\, f\, D] = x \sum_a e_a^2 \int d^2\boldsymbol{k}_\perp\, d^2\boldsymbol{p}_\perp\, \delta^{(2)}(z\boldsymbol{k}_\perp + \boldsymbol{p}_\perp - \boldsymbol{P}_{hT})\, w\left(\boldsymbol{k}_\perp, -\frac{\boldsymbol{p}_\perp}{z}\right) f^a(x, k_\perp^2)\, D_{h/a}(z, p_\perp^2),$$

(10)

or integrating over $d^2\boldsymbol{p}_\perp$:

$$\mathcal{C}[w\, f\, D] = x \sum_a e_a^2 \int d^2\boldsymbol{k}_\perp\; w\left(\boldsymbol{k}_\perp, -\frac{(\boldsymbol{P}_{hT} - z\boldsymbol{k}_\perp)}{z}\right) f^a(x, k_\perp^2)\, D_{h/a}\left(z, (\boldsymbol{P}_{hT} - z\boldsymbol{k}_\perp)^2\right).$$

(11)

For the sake of generality we use "f" and "D" functions to denote distribution and fragmentation TMD in formulas in this Section.

The kinematical functions, w, can be found in Refs. [5, 7, 48]. So-called moments of TMDs are defined accordingly as

$$f^{(n)a}(x) = \int d^2\boldsymbol{k}_\perp \left(\frac{k_\perp^2}{2M^2}\right)^n f^a(x, k_\perp^2)\,,$$

(12)

$$D_{h/a}^{(n)}(z) = \int d^2\boldsymbol{p}_\perp \left(\frac{p_\perp^2}{2z^2 M_h^2}\right)^n D_{h/a}(z, p_\perp^2)\,.$$

(13)

One also defines the "half" moment by

$$D_{h/a}^{(1/2)}(z) = \int d^2\boldsymbol{p}_\perp \frac{|p_\perp|}{2z M_h} D_{h/a}(z, p_\perp^2)\,.$$

(14)

Single Spin Asymmetry (SSA) measured experimentally is defined as:

$$A_{UT}^{\sin(3\phi_h - \phi_S)}(x, z, y, P_{hT}) \equiv \langle 2\sin(3\phi_h - \phi_S)\rangle = 2\frac{\int d\phi_h d\phi_S \sin(3\phi_h - \phi_S)\left(d\sigma^\uparrow - d\sigma^\downarrow\right)}{\int d\phi_h d\phi_S \left(d\sigma^\uparrow + d\sigma^\downarrow\right)}, \tag{15}$$

where $\uparrow (\downarrow)$ denote opposite transverse polarizations of the target nucleon, U stands for unpolarised lepton beam, T for the transverse polarization of the target nucleon. The numerator and denominator of Eq. (15) can be written as

$$d\sigma^\uparrow - d\sigma^\downarrow = \frac{\alpha^2 2 P_{hT}}{sx^2y^2} 2\left(1 - y\right)\sin(3\phi_h - \phi_S)\, F_{UT}^{\sin(3\phi_h - \phi_S)},$$

$$d\sigma^\uparrow + d\sigma^\downarrow = \frac{\alpha^2 2 P_{hT}}{sx^2y^2}\left(1 + (1 - y)^2\right) F_{UU,T}. \tag{16}$$

The final expression for $A_{UT}^{\sin(3\phi_h - \phi_S)}$ asymmetry reads

$$A_{UT}^{\sin(3\phi_h - \phi_S)}(x, z, y, P_{hT}) = \frac{\frac{\alpha^2 2 P_{hT}}{sx^2y^2}}{\frac{\alpha^2 2 P_{hT}}{sx^2y^2}} \cdot \frac{2\left(1 - y\right)}{(1 + (1 - y)^2)} \cdot \frac{F_{UT}^{\sin(3\phi_h - \phi_S)}}{F_{UU,T}}. \tag{17}$$

Note that $D_{NN} \equiv 2\left(1 - y\right)/(1 + (1 - y)^2)$ is often factored out from the measured asymmetry.

A. Unpolarised structure function, $F_{UU,T}$

The partonic interpretation of the unpolarised structure function $F_{UU,T}$ is the following [5, 7, 48]

$$F_{UU,T} = \mathcal{C}[f_1 D], \tag{18}$$

where f_1 and D are unpolarized TMD distribution and fragmentation functions. We have

$$F_{UU,T} = x\sum_{a=q,\bar{q}} e_a^2 \int d^2\mathbf{k}_\perp f_1^a(x, k_\perp^2) D_{h/a}\left(z, (\mathbf{P}_{hT} - z\mathbf{k}_\perp)^2\right). \tag{19}$$

Following Refs. [20, 51, 52] we assume Gaussian form for $f_1^a(x, k_\perp^2)$ and $D_{1h/a}(z, p_\perp^2)$:

$$f_1^a(x, k_\perp^2) = f_1^a(x)\frac{1}{\pi\langle k_\perp^2\rangle}\exp\left(-\frac{\mathbf{k}_\perp^2}{\langle k_\perp^2\rangle}\right),$$

$$D_{h/a}(z, p_\perp^2) = D_{h/a}(z)\frac{1}{\pi\langle p_\perp^2\rangle}\exp\left(-\frac{\mathbf{p}_\perp^2}{\langle p_\perp^2\rangle}\right). \tag{20}$$

Note that this is a correct representation of TMDs at tree level, as we mentioned in the Introduction we neglect possible effects coming from ressumation of soft gluons. The collinear distributions $f_1^a(x)$ and collinear fragmentation functions $D_{h/a}(z)$ in Eq. (20) will follow the usual DGLAP evolution in Q^2, we omit the explicit dependence on Q^2 in all formulas for simplicity.

Using Eqs. (19), (20) we obtain

$$F_{UU,T}(x, z, y, P_{hT}) = x\sum_{a=q,\bar{q}} e_a^2 f_1^a(x) D_{h/a}(z)\frac{1}{\pi\langle P_{hT}^2\rangle}\exp\left(-\frac{\mathbf{P}_{hT}^2}{\langle P_{hT}^2\rangle}\right), \tag{21}$$

where

$$\langle P_{hT}^2\rangle = \langle p_\perp^2\rangle + z^2\langle k_\perp^2\rangle. \tag{22}$$

Experimentally one can access $F_{UU,T}(x, z, y, P_{hT})$ by measuring unpolarized multiplicities of hadrons (pions, and kaons) in SIDIS. Recent analysis of unpolarized multiplicity data of HERMES collaboration [53] is presented Ref. [54] and analysis of data of HERMES [53] and COMPASS [55] collaborations is presented in Ref. [56]. Note that in principle, the widths of distribution and fragmentation functions $\langle k_\perp^2\rangle$ and $\langle p_\perp^2\rangle$ can be flavor dependent and can be functions of x and z correspondingly, however, for the sake of present analysis such dependencies are not very important and we will use a more simplified model [49] in which $\langle k_\perp^2\rangle = 0.25$ GeV^2 and $\langle p_\perp^2\rangle = 0.2$ GeV^2. In fact these values were used in extractions [20, 51, 52] of the Collins fragmentation functions that we will utilize in this paper.

B. Polarised structure function, $F_{UT}^{\sin(3\phi_h-\phi_S)}$

The partonic interpretation [5, 7, 48] of the structure function $F_{UT}^{\sin(3\phi_h-\phi_S)}$ involves the pretzelosity distribution ($h_{1T}^\perp$) and the so-called Collins fragmentation function ($H_1^\perp$):

$$F_{UT}^{\sin(3\phi_h-\phi_S)} = \mathcal{C}\left[\frac{-2\left(\hat{\boldsymbol{h}}\cdot\boldsymbol{p}_\perp\right)\left(\hat{\boldsymbol{h}}\cdot\boldsymbol{k}_\perp\right) - \boldsymbol{k}_\perp^2\left(\hat{\boldsymbol{h}}\cdot\boldsymbol{p}_\perp\right) + 4\left(\hat{\boldsymbol{h}}\cdot\boldsymbol{k}_\perp\right)^2\left(\hat{\boldsymbol{h}}\cdot\boldsymbol{p}_\perp\right)}{2M^2 M_h z}h_{1T}^\perp H_1^\perp\right], \tag{23}$$

where $\hat{\boldsymbol{h}} \equiv \boldsymbol{P}_{hT}/|\boldsymbol{P}_{hT}|$.

There exists a positivity bound [57] for $h_{1T}^{\perp a}$

$$\frac{\boldsymbol{k}_\perp^2}{2M^2}\left|h_{1T}^{\perp a}(x,k_\perp^2)\right| \le \frac{1}{2}(f_1^a(x,k_\perp^2) - g_1^a(x,k_\perp^2)). \tag{24}$$

We assume gaussian form for $g_1^q(x,k_\perp^2)$:

$$g_1^a(x,k_\perp^2) = g_1^a(x)\frac{1}{\pi\langle k_\perp^2\rangle}\exp\left(-\frac{\boldsymbol{k}_\perp^2}{\langle k_\perp^2\rangle}\right) , \tag{25}$$

where the width $\langle k_\perp^2\rangle = 0.25$ (GeV^2) is the same as for f_1^a. The widths could in principle be different, however given the precision of the experimental data, such an approximation is a reasonable one. The helicity distributions $g_1(x)$ are taken from Ref. [58], parton distributions $f_1(x)$ are the GRV98LO PDF set [59].

We assume the following form of $h_{1T}^{\perp a}$, that preserves the positivity bound of Eq. (24):

$$h_{1T}^{\perp a}(x,k_\perp^2) = \frac{M^2}{M_T^2}e^{-k_\perp^2/M_T^2}h_{1T}^{\perp a}(x)\frac{1}{\pi\langle k_\perp^2\rangle}\exp\left(-\frac{\boldsymbol{k}_\perp^2}{\langle k_\perp^2\rangle}\right) , \tag{26}$$

where

$$h_{1T}^{\perp a}(x) = e\mathcal{N}^a(x)(f_1^a(x) - g_1^a(x)),$$
$$\mathcal{N}^a(x) = N^a x^\alpha(1-x)^\beta\frac{(\alpha+\beta)^{\alpha+\beta}}{\alpha^\alpha\beta^\beta} , \tag{27}$$

where N^a, α, β, and M_T will be fitted to data, with $-1 \le N^a \le 1$.

We use Eq. (12) to calculate the first moment of $h_{1T}^{\perp a}(x,p_T^2)$ of Eq. (26) and obtain:

$$h_{1T}^{\perp(1)a}(x) = \frac{h_{1T}^{\perp a}(x)M_T^2\langle k_\perp^2\rangle}{2(M_T^2 + \langle k_\perp^2\rangle)^2} . \tag{28}$$

The parametrization of Collins fragmentation function $H_1^{\perp q}$ is taken from Refs. [20, 51, 52]:

$$H_{1h/a}^\perp(z,p_\perp) = \frac{zM_h}{2p_\perp}\Delta^N D_{h/a^\uparrow}(z,p_\perp) = \frac{zM_h}{M_C}e^{-p_\perp^2/M_C^2}H_{1h/a}^\perp(z)\frac{1}{\pi\langle p_\perp^2\rangle}\exp\left(-\frac{\boldsymbol{p}_\perp^2}{\langle p_\perp^2\rangle}\right) , \tag{29}$$

with

$$H_{1h/a}^\perp(z) = \sqrt{2e}\mathcal{N}_a^C(z)D_{h/a}(z),$$
$$\mathcal{N}_a^C(z) = N_a^C z^\gamma(1-z)^\delta\frac{(\gamma+\delta)^{(\gamma+\delta)}}{\gamma^\gamma\delta^\delta}, \tag{30}$$

where $-1 \le N_a^C \le 1$ and $\langle p_\perp^2\rangle = 0.2$ (GeV^2). The fragmentation functions (FF) $D_{h/a}(z)$ are from the DSS LO fragmentation function set [60]. Notice that with these choices the Collins fragmentation function automatically obeys its proper positivity bound [57]. In the fits we use the parameters of Collins FF obtained in Ref. [20]. Note that as in Ref. [20] we use two Collins fragmentation functions, *favored* and *unfavored* ones, see Ref. [20] for details on implementation, and corresponding parameters N_a^C are then N_{fav}^C and N_{unfav}^C.

According to Eq.(14) we obtain the following expression for the half moment of Collins fragmentation function:

$$H_{1h/a}^{\perp(1/2)}(z) = \frac{H_{1h/a}^\perp(z)M_C^2}{4}\sqrt{\frac{\pi\langle p_\perp^2\rangle}{(M_C^2 + \langle p_\perp^2\rangle)^3}} . \tag{31}$$

We also define the following variables:

$$\langle k_\perp^2 \rangle_T = \frac{\langle k_\perp^2 \rangle M_T^2}{\langle k_\perp^2 \rangle + M_T^2}, \ \langle p_\perp^2 \rangle_C = \frac{\langle p_\perp^2 \rangle M_C^2}{\langle p_\perp^2 \rangle + M_C^2},$$
$$\langle P_{hT}^2 \rangle_{CT} = \langle p_\perp^2 \rangle_C + z^2 \langle k_\perp^2 \rangle_T . \tag{32}$$

Polarized structure function $F_{UT}^{\sin(3\phi_h - \phi_S)}$ can be readily computed and reads (see also Ref. [48])

$$F_{UT}^{\sin(3\phi_h - \phi_S)}(x, z, y, P_{hT}) = \frac{xz^2 P_{hT}^3}{2} \sum_{a=q,\bar{q}} e_a^2 h_{1T}^{\perp(1)a}(x) H_{1h/a}^{\perp(1/2)}(z) \frac{\mathcal{C}}{\pi \langle P_{hT}^2 \rangle_{CT}^4} e^{-P_{hT}^2 / \langle P_{hT}^2 \rangle_{CT}} , \tag{33}$$

where

$$\mathcal{C} = 8 \langle k_\perp^2 \rangle_T \sqrt{\frac{\langle p_\perp^2 \rangle_C}{\pi}} . \tag{34}$$

One can see from Eq. (2) that under these assumptions on relation of pretzelosity to OAM we obtain

$$F_{UT}^{\sin(3\phi_h - \phi_S)} \propto \sum_q e_q^2 \mathcal{L}_z^q(x) . \tag{35}$$

Note that model relation of Eq.(2) is found to be valid only for quarks and not for anti-quarks, in this study we will neglect potential contributions from anti-quarks.

The experimental data are presented as sets of projections on x, z, and P_{hT}. In fact the three data sets are projection of the same dataset and not independent, thus in principle we should not include all sets in the fit[1]. However provided that the projections are at different average values of x, z, and P_{hT} we do gain sensitivity to distribution and fragmentation functions if we include simultaneously all three data sets. In the following we will assume them to be be independent and include them into our χ^2 analysis. However, it would be clearly beneficial for the phenomenological analysis if experiential data were presented in a simultaneous 4-D x, z, y, P_{hT} binning. For the asymmetry as a function of x, z we are using our result of Eq. (17) in particular the value of experimental point's $\langle P_{hT} \rangle$.

We also include a simplified scale dependence in the asymmetry by using Q^2 in the corresponding collinear distribution. The collinear quantities $h_{1T}^{\perp(1)a}(x)$ and $H_{1h/a}^{\perp(1/2)}(z)$ in general will be related to the so-called twist-3 matrix elements related to multy-parton correlations. Such matrix elements have a non-trivial QCD evolution (see for example Ref. [61]). The complete solutions of evolution equations are currently unknown and we substitute them by DGLAP evolution of corresponding collinear distributions in the parameterizations of Eqs. (27,30).

For completeness we give also results for P_{hT} integrated asymmetry

$$A_{UT}^{\sin(3\phi_h - \phi_S)}(x, z, y) = \frac{\frac{\alpha^2}{sx^2y^2} 2(1-y) \int dP_{hT} P_{hT} d\phi_h \ F_{UT}^{\sin(3\phi_h - \phi_S)}}{\frac{\alpha^2}{sx^2y^2} (1 + (1-y)^2) \int dP_{hT} P_{hT} d\phi_h \ F_{UU,T}} . \tag{36}$$

Using Eqs. (21),(33) we obtain

$$\int dP_{hT} P_{hT} d\phi_h \ F_{UU,T}(x, z, y, P_{hT}) = x \sum_{a=q,\bar{q}} e_a^2 f_1^a(x) D_{h/a}(z) ,$$
$$\int dP_{hT} P_{hT} d\phi_h \ F_{UT}^{\sin(3\phi_h - \phi_S)}(x, z, y, P_{hT}) = \frac{xz^2}{2} \sum_{a=q,\bar{q}} e_a^2 h_{1T}^{\perp(1)a}(x) H_{1h/a}^{\perp(1/2)}(z) \frac{3 \mathcal{C} \sqrt{\pi}}{4 \langle P_{hT}^2 \rangle_{CT}^{3/2}} . \tag{37}$$

P_{hT} integrated asymmetry was used for comparison with experimental results in Refs. [22, 23]. We checked explicitly that results of fitting with average values of $\langle P_{hT} \rangle$ and P_{hT} integrated ones are consistent with each other.

In the following we will use values of $\langle x \rangle$, $\langle y \rangle$, $\langle z \rangle$, $\langle P_{hT} \rangle$ in each experimental point to estimate the asymmetry using Eq. (33).

---

[1] We thank Gunar Schnell for discussion on this matter.

III. NULL SIGNAL HYPOTHESIS

Before proceeding to the phenomenology of pretzelosity, let us try to understand if the experimental data is compatible with a null hypothesis. We calculate the probability that $h_{1T}^{\perp a}(x, p_T^2) \equiv 0$ or $F_{UT}^{\sin(3\phi_h - \phi_S)} \equiv 0$.

We calculate thus the value of

$$\chi_0^2 = \sum_{n=1}^{N_{data}} \left(\frac{F_{UT}^{\sin(3\phi_h - \phi_S)}}{\Delta F_{UT}^{\sin(3\phi_h - \phi_S)}} \right)^2 , \tag{38}$$

where the experimental error is $\Delta F = \sqrt{\Delta F_{sys}^2 + \Delta F_{stat}^2}$.

Results are presented in Table. I. We see that the total value of $\chi^2 = 163.48$ for $N_{data} = 175$.

Experiment	hadron	Target	dependence	# ndata	χ^2	$\chi^2/ndata$
COMPASS [12]	h^+	LiD	x	9	2.12	0.23
COMPASS [12]	h^-	LiD	x	9	5.66	0.62
COMPASS [12]	h^+	LiD	z	8	15.45	1.93
COMPASS [12]	h^-	LiD	z	8	3.64	0.45
COMPASS [12]	h^+	LiD	P_{hT}	9	10.05	1.11
COMPASS [12]	h^-	LiD	P_{hT}	9	10.46	1.16
COMPASS [15]	h^+	NH$_3$	x	9	11.28	1.25
COMPASS [15]	h^-	NH$_3$	x	9	4.30	0.48
COMPASS [15]	h^+	NH$_3$	z	8	13.76	1.72
COMPASS [15]	h^-	NH$_3$	z	8	1.69	0.21
COMPASS [15]	h^+	NH$_3$	P_{hT}	9	11.12	1.24
COMPASS [15]	h^-	NH$_3$	P_{hT}	9	8.07	0.90
HERMES [16–18]	π^0	H	x	7	12.29	1.76
HERMES [16–18]	π^+	H	x	7	2.99	0.43
HERMES [16–18]	π^-	H	x	7	10.12	1.45
HERMES [16–18]	π^0	H	z	7	2.24	0.32
HERMES [16–18]	π^+	H	z	7	5.14	0.73
HERMES [16–18]	π^-	H	z	7	3.68	0.52
HERMES [16–18]	π^0	H	P_{hT}	7	5.74	0.82
HERMES [16–18]	π^+	H	P_{hT}	7	4.92	0.70
HERMES [16–18]	π^-	H	P_{hT}	7	12.89	1.84
JLAB [19]	π^+	^{3}He	x	4	4.35	1.19
JLAB [19]	π^-	^{3}He	x	4	1.52	0.41
				175	163.48	0.93

TABLE I. Results of analysis of null hypothesis

The goodness of this fit for a given χ^2 is normally calculated as $P(\chi^2, n_{d.o.f.})$, the integral of the probability distribution in χ^2 for $n_{d.o.f.}$ degrees of freedom, integrated from the observed minimum χ_0^2 to infinity:

$$P(\chi_0^2, n_{d.o.f.}) = 1 - \int_0^{\chi_0^2} d\chi^2 \frac{1}{2\Gamma(n_{d.o.f.}/2)} \left(\frac{\chi^2}{2} \right)^{n_{d.o.f.}/2 - 1} \exp\left[-\frac{\chi^2}{2} \right] \tag{39}$$

We obtain $P(163.48, 175) = 72\%$, i.e., there is a good chance that the quark-charge weighted sum over pretzelosity are zero or, in particular, all $h_{1T}^{\perp a}(x, p_T^2) = 0$. However we note that $F_{UT}^{\sin(3\phi_h - \phi_S)} \propto z^2 P_{h\perp}^3$ and thus asymmetry is suppressed by additional factor of $z P_{h\perp}^2$ with respect to Collins asymmetries, which were experimentally found to be non-zero. The latter do not usually exceed 10%. Assuming that $\langle z \rangle \sim 0.5$, $\langle P_{h\perp} \rangle \sim 0.5$ GeV, we conclude that even if $h_{1T}^{\perp a}(x, p_T^2)$ is of the same magnitude as the transversity distribution (that couples to Collins FF and generates Collins SSA), one would expect $F_{UT}^{\sin(3\phi_h - \phi_S)} \sim 1.5\%$ at most. In fact the maximum asymmetry due to pretzelosity was estimated to be order of $\sim 5\%$ in Ref. [23]. One can see that preliminary HERMES and COMPASS data are indeed in the range $|A_{UT}^{\sin(3\phi_h - \phi_S)}| \lesssim 2\%$, thus we will attempt fitting the data. We emphasize that future JLab 12 [2] data are going to be of extreme importance for exploring pretzelosity TMD in the valence quark region.

IV. PHENOMENOLOGY

In our analysis we are going to fit the unknown parameters for pretzelosity distributions. Provided the precision of the experimental data we are going to set α, β, and M_T to be flavor independent. We saw in the previous section that the data is compatible with zero pretzelosity and experimental errors are big. Therefore one is not able at present to determine all parameters and we will fix $\beta = 2$ as pretzelosity is expected [62–64] to be suppresed by $(1-x)^2$ with respect to unpolarised distribution. We also assume $\alpha_u = \alpha_d \equiv \alpha$. Thus we are going to fit 4 parameters: N_u, N_d, α, and M_T^2.

We will fit h^+ and h^- data and on effective deuteron (LiD) [12] and proton (NH$_3$) [15] targets from COMPASS collaboration, π^0, π^+, and π^- data on proton (H) target from preliminary HERMES [16–18], and JLab 6 data [19] on effective neutron (^{3}He) target.

Note that COMPASS data [12, 15] are presented in the following way:

$$A_{UT}^{\sin(3\phi_h - \phi_S)}{}_{COMPASS} = \frac{A_{UT}^{\sin(3\phi_h - \phi_S)}}{D_{NN}(\langle y \rangle)} \ , \tag{40}$$

where

$$D_{NN}(\langle y \rangle) = \frac{2(1 - \langle y \rangle)}{1 + (1 - \langle y \rangle)^2} \tag{41}$$

and $A_{UT}^{\sin(3\phi_h - \phi_S)}$ is from Eq.(17). In our fitting procedure we take $D_{NN}(\langle y \rangle)$ into account and use experimental values of $\langle y \rangle$ for each bin. The value of Q^2 is always set by the experiment and vary from bin to bin.

Parameters of Collins fragmentation function are taken from Ref. [20] and presented in Table II.

$$N_{fav}^C = 0.49_{-0.18}^{+0.2} \qquad N_{unfav}^C = -1_{-0}^{+0.38}$$
$$\gamma = 1.06_{-0.32}^{+0.45} \qquad \delta = 0.07_{-0.07}^{+0.42}$$
$$M_C^2 = 1.50_{-1.12}^{+2.00} \ (\text{GeV}^2)$$

TABLE II. Parameters of Collins FF, Ref. [20]

The resulting parameters after the fit are presented in Table. III and partial values of χ^2 are presented in Table. IV. One can easily see that the modern experimental data do not allow for a precise extraction of pretzelosity as the errors reported in Table. III are quite big. However, one notes that positive values for N_u and negative for N_d are preferred by the data.

In order to check which values of parameters are preferred by individual data sets we vary $N_u \in [-2, 2]$ and $N_d \in [-2, 2]$ and fix all other parameters to the best fit values. We calculate the total χ^2 and partial values of $\chi^2_{\text{COMPASS D}}$, $\chi^2_{\text{COMPASS P}}$, $\chi^2_{\text{HERMES P}}$, $\chi^2_{\text{JLAB N}}$ coming from data sets COMPASS [12], [15], HERMES [16–18], and JLab [19] . We then plot $\Delta\chi^2 \equiv \chi^2 - \chi^2_{min}$ as a function of N_u in Fig. 1 (a) and as a function of N_d in Fig. 1 (b). Here χ^2_{min} corresponds to the best fit. The point where all curves intersects correspond to the best fit value for $N_{u,d}$.

One can see from Fig. 1 that preliminary HERMES data prefer positive values for N_u and negative values for N_d and this tendency is the most prominent. COMPASS data, however, prefer negative values for N_u and positive values for N_d. The fit of all data sets in turn follows preference to positive values for N_u and negative values for N_d. The major part of the data come from the proton target, thus as expected, we have better determination of N_u due to up quark dominance and $\Delta\chi^2$ in fact is the biggest in this case (Fig. 1 (a)). We also expect that parameter N_d will be determined with bigger uncertainty (Fig. 1 (b)). One can also see from Fig. 1 that we cannot establish that pretzelosity does not violate positivity bounds, in fact values beyond region $[-1, 1]$ are also possible. We performed a study of possible positivity bound Eq. (24) violation by pretzelosity and found no evidence of such a violation in existing experimental data, in other words the fit does not yield values of N_u, N_d violating positivity bound if these parameters are allowed to vary in bigger region.

The errors of extraction are estimated using the monte carlo method from Ref. [65]. We generate 500 sets of parameters $\mathbf{a}_j = \{\alpha_j, N_{u\,j}, N_{d\,j}, M_{T\,j}^2\}$ that satisfy

$$\chi^2(\mathbf{a}_j) \leq \chi^2_{min} + \Delta\chi^2 \ , \tag{42}$$

where $\Delta\chi^2 = 9.72$ that corresponds for $P = 95.45\%$ of coverage probability for 4 parameters. Those parameter sets are then used to estimate the errors.

Resulting pretzelosity is presented in Fig. 2. One can see that resulting pretzelosity has very large error coridor and diminishes at small x. Future Jefferson Lab 12 GeV data is going to be crucial for the progress of phenomenology of
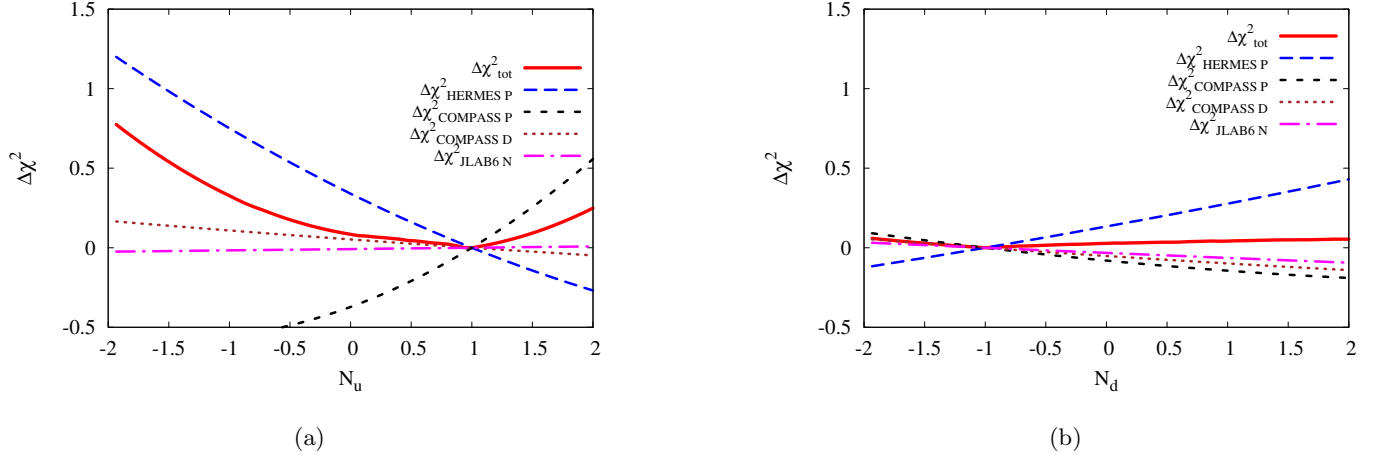
FIG. 1. $\Delta\chi^2$ as a function of N_u (a) and N_d (b) for total χ^2 and preliminary COMPASS [12], [15], HERMES [16–18], and JLab [19] separately.

α	$= 2.5 \pm 1.5$	β	$= 2$ fixed
N_u	$= 1 \pm 1.4$	N_d	$= -1 \pm 1.3$
M_T^2	$= 0.18 \pm 0.7$ (GeV^2)		
$\chi^2_{min} = 163.33$		$\chi^2_{min}/n.d.o.f = 0.95$	

TABLE III. Fitted parameters of the pretzelosity quark distributions.

the pretzelosity distribution as JLab 12 [2] data will explore high-x region. Fig. 2 also demonstrates that the best fit indicates positive pretzelosity for up quark and negative pretzelosity for down quark.
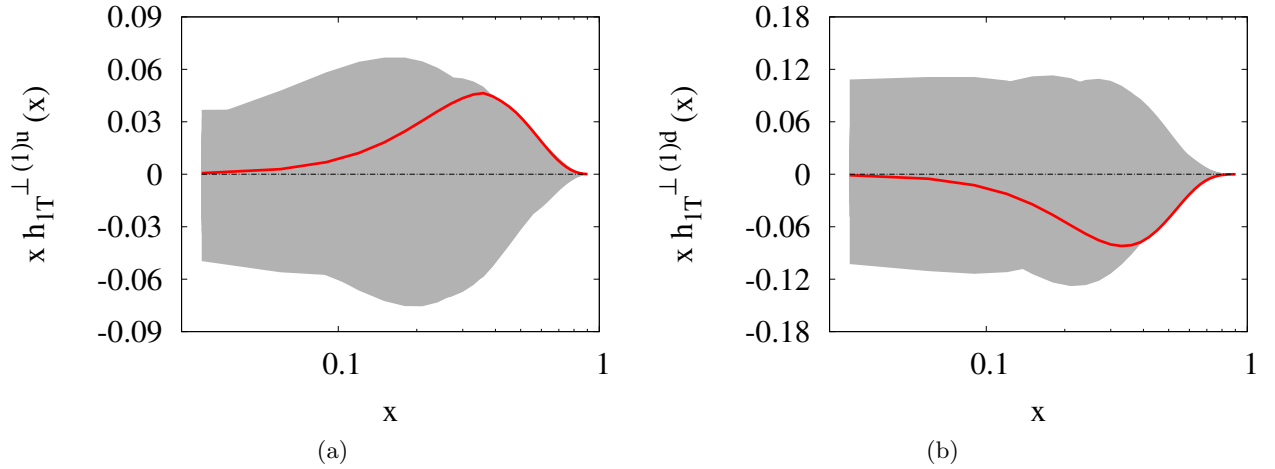
FIG. 2. First moment of the pretzelosity distribution for up (a) and down (b) quarks at $Q^2 = 2.4$ GeV^2. The solid line corresponds to the best fit and the shadowed region corresponds to the error corridor explained in the text.

We also plot in Fig. 3 the quadrupole modulation that corresponds to the pretzelosity distribution with particular choice of $\alpha = 1, \rho = 2$ from Eq. (1)

$$-\frac{1}{2}\frac{k_\perp^1 k_\perp^2}{M^2} x h_{1T}^\perp(x, k_\perp^2) \tag{43}$$

One can see from Fig. 3 that indeed quadrupole deformation of distribution is clearly present due to pretzelosity.

Results of description of COMPASS [12, 15] data on $h^\pm$ production are presented in Fig. 4 for proton (NH$_3$) target and in Fig. 5 for deuteron (LiD) target. One can see that expected asymmetry is very small especially

Experiment		hadron	Target	dependence	# ndata	χ^2	$\chi^2/ndata$
COMPASS [12]		h^+	LiD	x	9	2.11	0.23
COMPASS [12]		h^-	LiD	x	9	5.68	0.63
COMPASS [12]		h^+	LiD	z	8	15.45	1.93
COMPASS [12]		h^-	LiD	z	8	3.63	0.45
COMPASS [12]		h^+	LiD	P_{hT}	9	10.05	1.12
COMPASS [12]		h^-	LiD	P_{hT}	9	10.46	1.16
COMPASS [15]		h^+	NH$_3$	x	9	11.22	1.25
COMPASS [15]		h^-	NH$_3$	x	9	4.21	0.47
COMPASS [15]		h^+	NH$_3$	z	8	13.92	1.74
COMPASS [15]		h^-	NH$_3$	z	8	1.67	0.20
COMPASS [15]		h^+	NH$_3$	P_{hT}	9	11.23	1.25
COMPASS [15]		h^-	NH$_3$	P_{hT}	9	8.04	0.89
HERMES [16–18]	π^0	H	x	7	12.27	1.75
HERMES [16–18]	π^+	H	x	7	3.05	0.44
HERMES [16–18]	π^-	H	x	7	10.06	1.44
HERMES [16–18]	π^0	H	z	7	2.23	0.32
HERMES [16–18]	π^+	H	z	7	5.08	0.73
HERMES [16–18]	π^-	H	z	7	3.47	0.50
HERMES [16–18]	π^0	H	P_{hT}	7	5.74	0.82
HERMES [16–18]	π^+	H	P_{hT}	7	4.84	0.69
HERMES [16–18]	π^-	H	P_{hT}	7	12.93	1.85
JLAB [19]		π^+	^{3}He	x	4	4.35	1.09
JLAB [19]		π^-	^{3}He	x	4	1.56	0.39
					175	163.33	0.93

TABLE IV. Partial χ^2 values of the best fit.
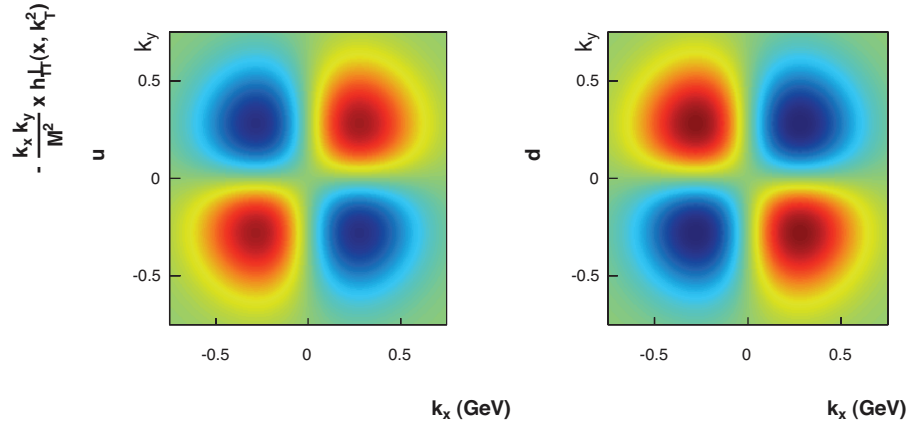
FIG. 3. Tomographic slice of the pretzelosity distribution Eq. (43) at $x = 0.1$ for up and down quarks. Red color mean positive sign function while blue color mean negative sign function.

for z and P_{hT} dependence, the reason is that COMPASS $\langle x \rangle \simeq 0.03$ is quite small and pretzelosity quickly diminishes at small x. However error corridor is quite large. In addition, cancellation of u and d pretzelosities makes asymmetries on deuteron target vanishing, see Fig. 5. Indeed for h^+ production on deuteron target $F_{UT}^{\sin(3\phi_h - \phi_S)} \propto 4(h_{1T}^{\perp u} + h_{1T}^{\perp d})H_1^{\perp fav} + (h_{1T}^{\perp u} + h_{1T}^{\perp d})H_1^{\perp unfav} \sim 0$ as far as our result indicates that $h_{1T}^{\perp u} + h_{1T}^{\perp d} \sim 0$. Overall smallness of asymmetry on the proton target in Fig. 4 is due to the suppression factor $z^2 P_{hT}^3$. Our result also indicates that pretzelosity diminishes as x becomes smaller, thus we have almost vanishing results for small values of x. We cannot of course exclude possible contribution from sea quarks or bigger values of pretzelosity in small-x region. Note that our results are scaled by D_{NN} in order to be compared to the COMPASS data .
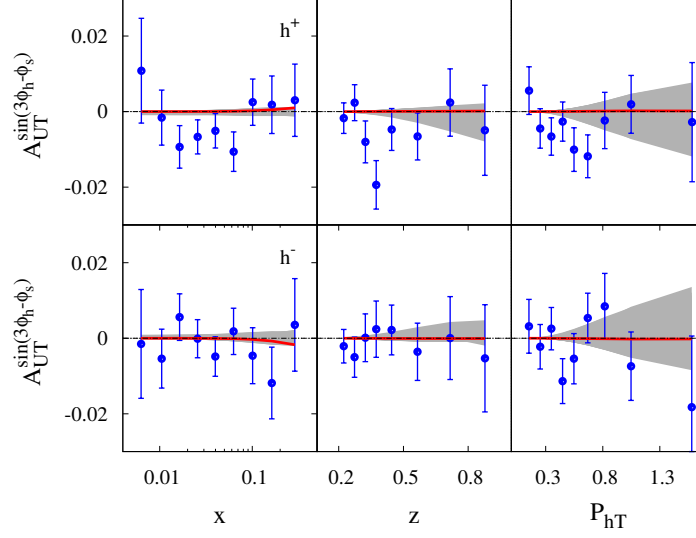
FIG. 4. $A_{UT}^{\sin(3\phi_h-\phi_S)}$ measured by COMPASS Collaboration on proton (NH$_3$) target [15] as a function of x, z, P_{hT} for h^+ and h^-. The solid line corresponds to the best fit and the shadowed region corresponds to the error corridor.
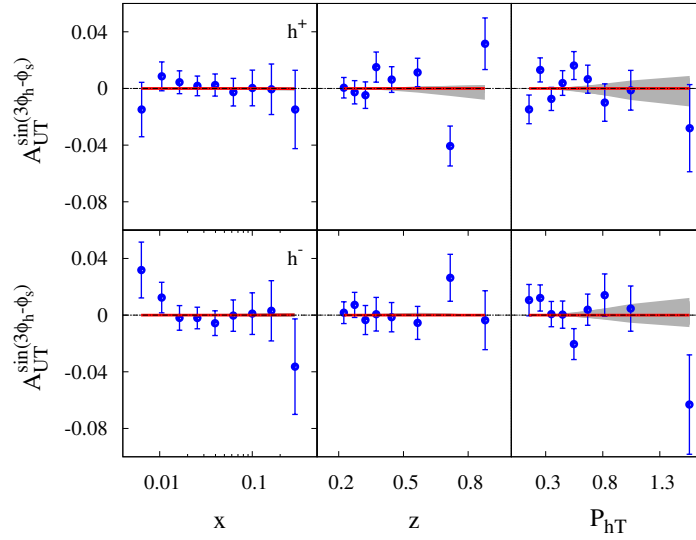

FIG. 5. $A_{UT}^{\sin(3\phi_h-\phi_S)}$ measured by COMPASS Collaboration on deuteron (LiD) target [12] as a function of x, z, P_{hT} for h^+ and h^-. The solid line corresponds to the best fit and the shadowed region corresponds to the error corridor.

The results of the description of preliminary experimental HERMES [16–18] data for π^+ and π^- production on proton target are presented in Fig. 6. Note that schematically for π^+ production on the proton target $F_{UT}^{\sin(3\phi_h-\phi_S)} \propto 4h_{1T}^{\perp u}H_1^{\perp fav} + h_{1T}^{\perp d}H_1^{\perp unfav}$ and as far as our result indicates that $h_{1T}^{\perp u}H_1^{\perp fav} > 0$ and $h_{1T}^{\perp d}H_1^{\perp unfav} > 0$, the asymmetry is effectively enhanced and positive for π^+. Similarly for π^- we have $F_{UT}^{\sin(3\phi_h-\phi_S)} \propto 4h_{1T}^{\perp(1)u}H_1^{\perp(1/2)unfav} + h_{1T}^{\perp(1)d}H_1^{\perp(1/2)fav} < 0$.

The smallness of the asymmetry in Fig. 6 is explained by suppression factor $z^2 P_{hT}^3$, as far as the average values of HERMES are $\langle z \rangle \simeq 0.36$ and $\langle P_{hT} \rangle \simeq 0.4$ (GeV) and thus $z^2 P_{hT}^3 \simeq 0.008$ (GeV^3). This makes possible values of the asymmetry be well below 1%.

Fit of the neutron data on $\pi^\pm$ production from JLab 6 [19] is shown in Fig. 7. The sign of the asymmetry for π^+ is negative, as on neutron $F_{UT}^{\sin(3\phi_h-\phi_S)} \propto 4h_{1T}^{\perp d}H_1^{\perp fav} + h_{1T}^{\perp u}H_1^{\perp unfav} < 0$ and positive for π^- as $F_{UT}^{\sin(3\phi_h-\phi_S)} \propto$
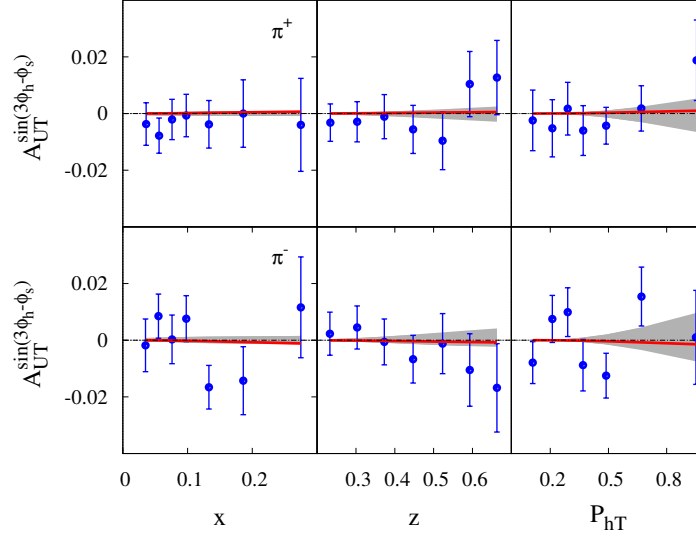
FIG. 6. Preliminary HERMES [16–18] results on $A_{UT}^{\sin(3\phi_h-\phi_S)}$ as a function of x, z, P_{hT} for π^+ and π^-. The solid line corresponds to the best fit and the shadowed region corresponds to the error corridor.

$4h_{1T}^{\perp d}H_1^{\perp unfav} + h_{1T}^{\perp u}H_1^{\perp fav} > 0$. Due to kinematical suppression the resulting asymmetry is very small, the measured asymmetry has very big errors and is compatible with out fit.
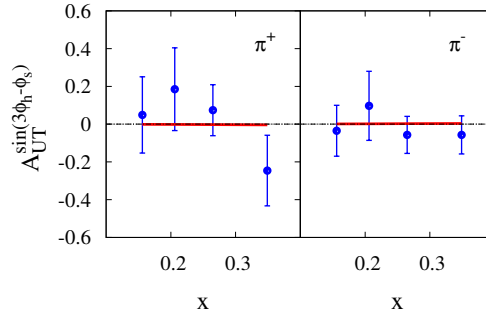

FIG. 7. $A_{UT}^{\sin(3\phi_h-\phi_S)}$ measured by JLab [19] on neutron (^{3}He) target as a function of x for π^+ (left panel) and π^- (right panel). The solid line corresponds to the best fit and the shadowed region corresponds to the error corridor.

A. Predictions for Jefferson Lab 12 GeV

We present predictions for future measurements of $A_{UT}^{\sin(3\phi_h-\phi_S)}$ on proton target at Jefferson Lab at 12 GeV in Fig. 8. We plot our prediction for π^+ production on proton target assuming $\langle z \rangle = 0.5$ and $\langle P_{hT} \rangle = 0.38$ GeV. We predict absolute value of the asymmetry of order of 1%. Both positive and negative asymmetries are possible, current data prefer positive asymmetry for π^+ on the proton target (positive u quark pretzelosity times positive favored Collins FF) and negative asymmetry for π^- (positive u quark pretzelosity times negative unfavored Collins FF). Signs of asymmetries on neutron target are reversed with respect to the proton target and absolute values are slightly higher.
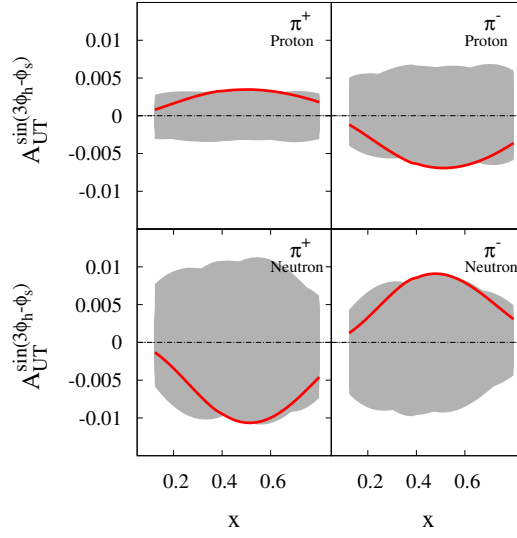
FIG. 8. Prediction of $A_{UT}^{\sin(3\phi_h - \phi_S)}$ at JLab 12 kinematics on proton (upper two plots) and neutron (bottom two plots) targets as a function of x for π^+ (left panels) and π^- (right panels). The solid line corresponds to the best fit and the shadowed region corresponds to the error corridor.

V. COMPARISON WITH OTHER CALCULATIONS

Our results are of opposite sign if compared to model calculations of [21–27]. Most models predict that $h_{1T}^{\perp u} < 0$ and $h_{1T}^{\perp d} > 0$ while our best fit indicates that $h_{1T}^{\perp u} > 0$ and $h_{1T}^{\perp d} < 0$. However as can be seen from Fig. 2 our fit does not give a clear preference on the sign of pretzelosity.

The size of asymmetries is compatible with calculations of Ref. [22], where asymmetries of order of 1% for π^+ and 0.5% for π^- were found for JLab kinematics and can be compared to our findings in Fig. 8. Other calculations, for example [21] or [23] suggest bigger asymmetries up to 4-5% for COMPASS kinematics and 2-5% for JLab 12 kinematics. In contrast our calculations suggest that asymmetry at JLab 12 will be of order of 1% at most. Future experimental measurements will be very important to clarify the sign and the size of pretzelosity and $A_{UT}^{\sin(3\phi_h - \phi_S)}$ asymmetry.

VI. MODEL RELATIONS AND BOUNDS FOR PRETZELOSITY

Positivity bound for the pretzelosity reads [57]

$$\left| h_{1T}^{\perp(1)a}(x) \right| \leq \frac{1}{2} (f_1^a(x) - g_1^a(x)) . \tag{44}$$

If combined with Soffer bound $h_1^a(x) \leq 1/2(f_1^a(x) + g_1^a(x))$ [66] one obtains [23]

$$|h_1^a(x)| + \left| h_{1T}^{\perp(1)a}(x) \right| \leq f_1^a(x) . \tag{45}$$

In a certain class of models including bag models (see, e.g., [23]) one obtains also the following model relations for the pretzelosity and transversity:

$$2h_1^a(x) = f_1^a(x) + g_1^a(x) , \tag{46}$$

$$h_{1T}^{\perp(1)a}(x) = h_1^a(x) - f_1^a(x) . \tag{47}$$

or

$$h_{1T}^{\perp(1)a}(x) = g_1^a(x) - h_1^a(x) . \tag{48}$$

Let us examine these model relations. Eq. (47) implies that transversity saturates the Soffer bound [66]. In fact we know that phenomenological extraction of transversity is close to the bound, however the bound is not saturated,
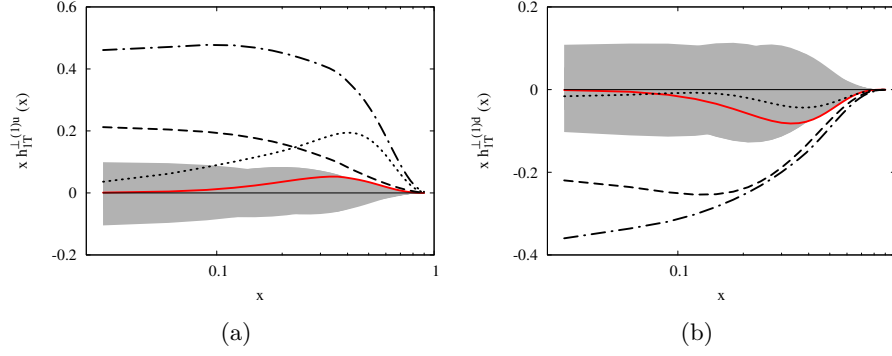
FIG. 9. First moment of the pretzelosity distribution for up (a) and down (b) quarks. The red solid line corresponds to the best fit and the shadowed region corresponds to the error corridor. Dotted line is model relation Eq. (48) $h_{1T}^{\perp(1)a}(x) = g_1^a(x) - h_1^a(x)$, thick dashed line is positivity bound Eq. (44) $\pm|\frac{1}{2}(f_1^a(x) - g_1^a(x))|$, and the alternating dashed and dotted line is bound from Eq. (45) $\pm|f_1^a(x) - |h_1^a(x)||$. Neither of bounds is violated.

see e.q. Ref. [65] . If the bound were saturated, then Eqs. (47,48) would simply read:

$$h_{1T}^{\perp(1)a}(x) = \frac{1}{2}(g_1^a(x) - f_1^a(x)) \,, \tag{49}$$

i.e. positivity bound for pretzelosity would be saturated as well.

   In order to compare these model predictions with our results we plot in Fig. 9 first moment of pretzelosity for up and down quarks and results from Eq. (48) using transversity from Ref. [65] (dotted line) and positivity bound (44) (thick dashed line). One can see that if one uses extracted transversity in Eq. (48) then resulting pretzelosity violates the positivity bound. We also plot $f_1^a(x) - |h_1^a(x)|$ (dot dashed lines). One can see that neither of positivity bounds Eqs.(44), (45) is violated by our extracted pretzelosity. Model relation of Eq. (48) does violate one of the positivity bounds if transversity does not saturate Soffer bound. Numerical comparison of Eq. (48) with extracted pretzelosity suggest that for up quark there is a big discrepancy, in fact our parameterization is constructed to satisfy positivity bound while Eq. (48) may violate it (compare Eq. (49) that assumes saturation of bounds and model relation of Eq. (48)). For down quark comparison is better, numerically results are similar, in this case model relation Eq. (48) numerically satisfies the bound. We also checked that if one fits the data without imposing positivity constraints by construction when extracted first moment of pretzelosity does not violate positivity bound in the region of x where experimental data are available, $0.0065 < x < 0.35$. At large values of x violation is possible, however this region is not constrained by the data.

VII.   QUARK ORBITAL ANGULAR MOMENTUM

Using the pretzelosity from the previous section let us calculate quark OAM in the region of experimental data $0.0065 \leq x \leq 0.35$

$$\mathcal{L}_z^{a[x_{min},x_{max}]} = -\int_{x_{min}}^{x_{max}} dx \, h_{1T}^{\perp(1)a}(x, Q^2) \,. \tag{50}$$

Using the parameters with errors from Table III we calculate the following values at $Q^2 = 2.4$ GeV^2:

$$\mathcal{L}_z^{u[0.0065,0.35]} = -0.03_{-0.10}^{+0.25} \,,$$
$$\mathcal{L}_z^{d[0.0065,0.35]} = +0.05_{-0.34}^{+0.49} \,. \tag{51}$$

If we integrate over the whole kinematical region $0 < x < 1$ then we obtain

$$\mathcal{L}_z^{u[0,1]} = -0.06_{-0.10}^{+0.38} \,,$$
$$\mathcal{L}_z^{d[0,1]} = +0.08_{-0.60}^{+0.93} \,. \tag{52}$$

One notes that substantial value of the integral comes from unexplored high-x and low-x regions.

VIII. CONCLUSIONS

We performed the first extraction of the pretzelosity distribution from preliminary COMPASS, HERMES, and JLab experimental data. Even though the present extraction has big errors we conclude that up quark pretzelosity tends to be positive and down quark pretzelosity tends to be negative. This conclusion is not in agreement with models [21–27] that predict negative up quark pretzelosity and positive down quark pretzelosity. We note that extracted pretzelosity has very big errors and allow for both positive and negative signs. Indeed, a vanishing asymmetry is well consistent with existing experimental data. Future experimental data from Jefferson Lab 12 [2] will be essential for determination of properties of the pretzelosity distribution.

The extracted pretzelosity can be related in a model dependent way to quark OAM and at $Q^2 = 2.4$ GeV^2 $\mathcal{L}_z^{u[0,1]} = -0.06^{+0.38}_{-0.10}$, $\mathcal{L}_z^{d[0,1]} = +0.08^{+0.93}_{-0.60}$.

ACKNOWLEDGMENTS

[1] J.-C. Peng and J.-W. Qiu, Prog.Part.Nucl.Phys. **76**, 43 (2014), arXiv:1401.0934.
[2] J. Dudek *et al.*, Eur.Phys.J. **A48**, 187 (2012), arXiv:1208.1244.
[3] A. Accardi *et al.*, (2012), arXiv:1212.1701.
[4] G. A. Miller, Phys.Rev. **C68**, 022201 (2003), arXiv:nucl-th/0304076.
[5] P. J. Mulders and R. D. Tangerman, Nucl. Phys. **B461**, 197 (1996), arXiv:hep-ph/9510301.
[6] K. Goeke, A. Metz, and M. Schlegel, Phys. Lett. **B618**, 90 (2005), arXiv:hep-ph/0504130.
[7] A. Bacchetta *et al.*, JHEP **02**, 093 (2007), hep-ph/0611265.
[8] J. P. Ralston and D. E. Soper, Nucl. Phys. **B152**, 109 (1979).
[9] D. Boer and P. J. Mulders, Phys. Rev. **D57**, 5780 (1998), arXiv:hep-ph/9711485.
[10] A. Kotzinian and P. Mulders, Phys.Lett. **B406**, 373 (1997), arXiv:hep-ph/9701330.
[11] J. C. Collins, Nucl. Phys. **B396**, 161 (1993).
[12] COMPASS Collaboration, B. Parsamyan, Eur.Phys.J.ST **162**, 89 (2008), arXiv:0709.3440.
[13] B. Parsamyan, J.Phys.Conf.Ser. **295**, 012046 (2011), arXiv:1012.0155.
[14] B. Parsamyan, (2013), arXiv:1301.6615.
[15] B. Parsamyan, (2013), arXiv:1307.0183.
[16] HERMES Collaboration, M. Diefenthaler, talk delivered at the topical pre-workshop 'Partonic transverse momentum distributions' at EINN 2009 (2009).
[17] HERMES Collaboration, G. Schnell, PoS **DIS2010**, 247 (2010).
[18] HERMES Collaboration, L. Pappalardo, p. 312 (2010).
[19] Jefferson Lab Hall A Collaboration, Y. Zhang *et al.*, (2013), arXiv:1312.3047.
[20] M. Anselmino *et al.*, Phys.Rev. **D87**, 094019 (2013), arXiv:1303.3822.
[21] A. Kotzinian, (2008), arXiv:0806.3804.
[22] J. She, J. Zhu, and B.-Q. Ma, Phys.Rev. **D79**, 054008 (2009), arXiv:0902.3718.
[23] H. Avakian, A. Efremov, P. Schweitzer, and F. Yuan, Phys.Rev. **D78**, 114024 (2008), arXiv:0805.3355.
[24] B. Pasquini, S. Cazzaniga, and S. Boffi, Phys.Rev. **D78**, 034025 (2008), arXiv:0806.2298.
[25] B. Pasquini, S. Boffi, and P. Schweitzer, Mod.Phys.Lett. **A24**, 2903 (2009), arXiv:0910.1677.
[26] S. Boffi, A. Efremov, B. Pasquini, and P. Schweitzer, Phys.Rev. **D79**, 094012 (2009), arXiv:0903.1271.
[27] H. Avakian, A. Efremov, P. Schweitzer, and F. Yuan, Phys.Rev. **D81**, 074035 (2010), arXiv:1001.5467.
[28] A. Efremov, P. Schweitzer, O. Teryaev, and P. Zavada, PoS **DIS2010**, 253 (2010), arXiv:1008.3827.
[29] C. Lorce and B. Pasquini, Phys.Lett. **B710**, 486 (2012), arXiv:1111.6069.
[30] LHPC Collaborations, P. Hagler *et al.*, Phys.Rev. **D77**, 094502 (2008), arXiv:0705.4295.
[31] S. Syritsyn *et al.*, PoS **LATTICE2011**, 178 (2011), arXiv:1111.0718.
[32] K. Liu *et al.*, PoS **LATTICE2011**, 164 (2011), arXiv:1203.6388.
[33] X.-D. Ji, Phys.Rev.Lett. **78**, 610 (1997), arXiv:hep-ph/9603249.
[34] M. Deka *et al.*, (2013), arXiv:1312.4816.
[35] D. W. Sivers, Phys.Rev. **D41**, 83 (1990).

[36] S. J. Brodsky, D. S. Hwang, and I. Schmidt, Nucl. Phys. **B642**, 344 (2002), arXiv:hep-ph/0206259.
[37] J. C. Collins, Phys. Lett. **B536**, 43 (2002), hep-ph/0204004.
[38] Z.-B. Kang and J.-W. Qiu, Phys.Rev.Lett. **103**, 172001 (2009), arXiv:0903.3629.
[39] M. Buffing, A. Mukherjee, and P. Mulders, Phys.Rev. **D86**, 074030 (2012), arXiv:1207.3221.
[40] S. Meissner, A. Metz, and M. Schlegel, JHEP **0908**, 056 (2009), arXiv:0906.5323.
[41] R. Jaffe and A. Manohar, Nucl.Phys. **B337**, 509 (1990).
[42] C. Lorce and B. Pasquini, Phys.Rev. **D84**, 014015 (2011), arXiv:1106.0139.
[43] H. BC and M. Burkardt, Few Body Syst. **52**, 389 (2012), arXiv:1103.0028.
[44] K. Kanazawa, C. Lorc, A. Metz, B. Pasquini, and M. Schlegel, (2014), arXiv:1403.5226.
[45] A. Mukherjee, S. Nair, and V. K. Ojha, (2014), arXiv:1403.6233.
[46] A. Courtoy, G. R. Goldstein, J. O. G. Hernandez, S. Liuti, and A. Rajan, Phys.Lett. **B731**, 141 (2014), arXiv:1310.5157.
[47] M. Burkardt and H. BC, Phys.Rev. **D79**, 071501 (2009), arXiv:0812.1605.
[48] M. Anselmino *et al.*, Phys.Rev. **D83**, 114019 (2011), arXiv:1101.1011.
[49] M. Anselmino, M. Boglione, A. Prokudin, and C. Turk, Eur. Phys. J. **A31**, 373 (2007), arXiv:hep-ph/0606286.
[50] D. Boer *et al.*, (2011), arXiv:1108.1713.
[51] M. Anselmino *et al.*, Nucl. Phys. Proc. Suppl. **191**, 98 (2009), arXiv:0812.4366.
[52] M. Anselmino *et al.*, Phys. Rev. **D75**, 054032 (2007), arXiv:hep-ph/0701006.
[53] HERMES Collaboration, A. Airapetian *et al.*, Phys.Rev. **D87**, 074029 (2013), arXiv:1212.5407.
[54] A. Signori, A. Bacchetta, M. Radici, and G. Schnell, (2013), arXiv:1309.3507.
[55] COMPASS, C. Adolph *et al.*, Eur.Phys.J. **C73**, 2531 (2013), arXiv:1305.7317.
[56] M. Anselmino, M. Boglione, J. Gonzalez H., S. Melis, and A. Prokudin, JHEP **1404**, 005 (2014), arXiv:1312.6261.
[57] A. Bacchetta, M. Boglione, A. Henneman, and P. J. Mulders, Phys. Rev. Lett. **85**, 712 (2000), arXiv:hep-ph/9912490.
[58] D. de Florian, R. Sassot, M. Stratmann, and W. Vogelsang, Phys.Rev. **D80**, 034030 (2009), arXiv:0904.3821.
[59] M. Gluck, E. Reya, and A. Vogt, Eur. Phys. J. **C5**, 461 (1998), arXiv:hep-ph/9806404.
[60] D. de Florian, R. Sassot, and M. Stratmann, Phys. Rev. **D75**, 114010 (2007), arXiv:hep-ph/0703242.
[61] Z.-B. Kang, J.-W. Qiu, and W. Vogelsang, Phys.Rev. **D79**, 054007 (2009), arXiv:0811.3662.
[62] H. Avakian, S. J. Brodsky, A. Deur, and F. Yuan, Phys.Rev.Lett. **99**, 082001 (2007), arXiv:0705.1553.
[63] S. J. Brodsky and F. Yuan, Phys.Rev. **D74**, 094018 (2006), arXiv:hep-ph/0610236.
[64] M. Burkardt, (2007), arXiv:0709.2966.
[65] M. Anselmino *et al.*, Eur.Phys.J. **A39**, 89 (2009), arXiv:0805.2677.
[66] J. Soffer, Phys. Rev. Lett. **74**, 1292 (1995).